Growing quantum states with topological order

Fabian Letscher,[1,2] Fabian Grusdt,[1,2] and Michael Fleischhauer[1]
[1]*Department of Physics and Research Center OPTIMAS, University of Kaiserslautern, Germany*
[2]*Graduate School Materials Science in Mainz, Gottlieb-Daimler-Strasse 47, 67663 Kaiserslautern, Germany*
(Received 24 February 2015; revised manuscript received 7 May 2015; published 26 May 2015)

We discuss a protocol for growing states with topological order in interacting many-body systems using a sequence of flux quanta and particle insertion. We first consider a simple toy model, the superlattice Bose-Hubbard model, to explain all required ingredients. Our protocol is then applied to fractional quantum Hall systems in both, continuum and lattice. We investigate in particular how the fidelity, with which a topologically ordered state can be grown, scales with increasing particle number N. For small systems, exact diagonalization methods are used. To treat large systems with many particles, we introduce an effective model based on the composite fermion description of the fractional quantum Hall effect. This model also allows to take into account the effects of dispersive bands and edges in the system, which will be discussed in detail.

DOI: 10.1103/PhysRevB.91.184302 PACS number(s): 67.85.−d, 73.43.−f, 03.65.Vf

I. INTRODUCTION

Since the discovery of the integer quantum Hall effect (IQHE) in 1980 [1] and two years later the fractional quantum Hall effect (FQHE) [2], the interest in states exhibiting topological order has increased tremendously. Due to their robustness against local disorder, these states are for instance well suited for metrology [1]. Another interesting aspect of such interacting many-body systems is that they host states with anyonic excitations [3–5]. In this context, non-Abelian anyons are particularly exciting because they can be employed to build a topological quantum computer [6], if they can be coherently manipulated.

For many years, solid state systems with electrons appeared to be the only candidates to realize exotic many-body states, e.g., in the FQHE. However, their small intrinsic length scales make coherent control difficult. On the other hand, the rapid development of ultracold gases and photonic systems is a promising route to implement various Hamiltonians known from the solid state community, with full coherent control. With the current state of the art technology, noninteracting topological states have been observed in ultracold gases [7–10] as well as photonic systems [11,12].

Unlike in the solid state context, efficient cooling mechanisms below the many-body gap are still lacking in systems of interacting atoms and photons, which makes the preparation of topological states challenging. In this paper, we develop an alternative dynamical scheme for the efficient preparation of highly correlated ground states with topological order. It can be implemented with ultracold atoms or photons and exploits the coherent control techniques available in these systems.

To solve the cooling problem, different approaches were discussed previously. In Ref. [13], it was suggested to pump the sites of a dissipative lattice system coherently. This scheme relies on a direct N-photon transition and thus works only for small systems. Moreover, the state prepared is in a superposition of different particle numbers. Another proposal [14] suggested to rapidly refill the hole excitations due to local loss in a lattice system. This protocol stabilizes the ground state dynamically.

In Ref. [15], we proposed a scheme to grow the highly correlated Laughlin states. Here, we discuss the general ingredients of the protocol, which may also be used to grow other topological ordered states in interacting many-body systems. To do so, we consider a simple toy model explaining all necessary ingredients. The main ideas of the protocol can be summarized as follows. In the first step, a topologically protected and quantized Thouless pump [16,17] is used to create a localized hole excitation in the system. In the second step, the hole is refilled using a coherent pump. Local repulsive interactions between the particles are employed to provide a blockade mechanism such that only a single particle is inserted. In the case of the FQHE, we analyze the performance of the protocol in detail and explain how the fidelity scales with the particle number N. In order to treat large fractional Chern insulator systems with many particles, we introduce an effective model based on the composite fermion (CF) description of the FQHE. Within this model, we are able to demonstrate, that the growing scheme still works despite the presence of gapless edge states and dispersive bands in large lattice systems. As shown in Fig. 1, we reach a homogeneous density in the bulk with an average CF magnetic filling factor $\nu^* \simeq 0.9$, close to the optimal value $\nu^* = 1$.

The paper is structured as follows. We start by describing the growing scheme using a simple toy model in Sec. II. In Sec. III, we discuss the protocol in a FQH system. Moreover, we discuss the performance of the protocol. The Sec. IV considers fractional Chern insulators. There, we discuss edge and band dispersion effects based on our effective CF model. In Sec. V, we summarize the results and give a short outlook.

II. TOPOLOGICAL GROWING SCHEME

In this section, we discuss the basic idea how states with topological order can be grown for the one-dimensional superlattice Bose Hubbard model (SLBHM) as a toy model. This sets the stage for the following discussions of two-dimensional systems with topological order.

A. Toy model

The SLBHM can be used to implement a quantized pump [16–19], which can be related to a nontrivial topological

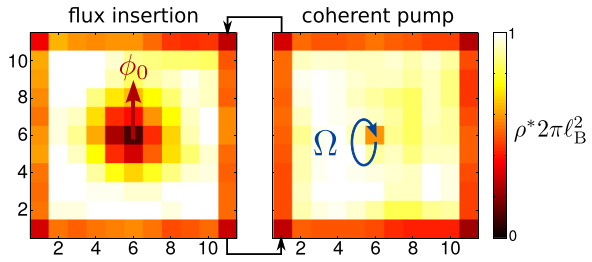

FIG. 1. (Color online) Simulation of the effective composite fermion (CF) lattice model. The figure shows the CF density ρ^* of a lattice with 11×11 sites and effective flux per plaquette $\alpha^* = 0.1$. The basic ingredients of the protocol are (i) flux insertion, which creates a CF quasihole excitation and (ii) a coherent CF pump, which refills the hole excitation. Additionally, we include a quasihole trapping potential ($g_h = 1J^*$) and absorbing boundaries ($\gamma_{\text{Edge}} = 0.0025J^*$) to account for the effects of dispersive bands and edge states.

invariant. The Hamiltonian of the SLBHM is

$$\hat{\mathcal{H}} = -J_1 \sum_j (\hat{a}_j^\dagger \hat{b}_j + \text{H.c.}) - J_2 \sum_j (\hat{a}_j^\dagger \hat{b}_{j+1} + \text{H.c.}) + \delta \sum_j \hat{b}_j^\dagger \hat{b}_j + U/2 \sum_j (\hat{a}_j^\dagger \hat{a}_j^\dagger \hat{a}_j \hat{a}_j + \hat{b}_j^\dagger \hat{b}_j^\dagger \hat{b}_j \hat{b}_j), \quad (1)$$

where $\hat{a}_j(\hat{b}_j)$ annihilates a boson on lattice site A (B) in the jth unit cell [see Fig. 2(a)]. Note that we consider here a semi-infinite system with an open boundary on the left. The hopping elements are denoted by J_1, J_2, while δ is an on-site potential shift acting on lattice sites B. Furthermore, we include on-site interactions U for more than one particle per site.

In the case of vanishing δ and disregarding interactions, the different hopping amplitudes $J_1 \neq J_2$ determine the dimerization of the two sites A and B in the unit cell. This leads to a two-band model with a band gap E_{gap} and bandwidth ΔE determined by the ratio J_2/J_1. In the limit $J_2/J_1 \to 0$, the flatness ratio $E_{\text{gap}}/\Delta E$ tends to infinity and the two bands become nondispersive. At filling $\rho = 1/2$ and with interactions, the ground state of the system is a Mott insulator (MI) with many-body gap Δ or a superfluid (SF) depending on the specific parameters J_2/J_1 and U [20–23]. Specifically, for large interactions U, the model can be mapped to free fermions. The resulting ground state at $\rho = 1/2$ is incompressible whenever $J_1 \neq J_2$ or $|\delta| \neq 0$. For finite interaction U, the SF region is extended in parameter space $(J_1 - J_2, \delta)$ as depicted in Fig. 2(b).

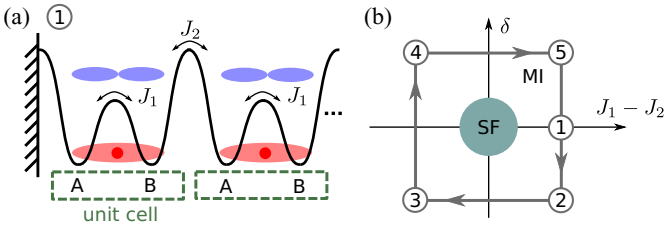

FIG. 2. (Color online) (a) Semi-infinite chain of coupled dimers, consisting of two sites A, B. Initially, the MI ground state is prepared with filling $\rho = 1/2$. (b) Schematic phase diagram of the SLBHM in the regime of intermediate interactions U. Following adiabatically the loop 1-5 corresponds to a Thouless pump: Encircling the SF region, all particles in the MI are shifted one dimer to the right.

B. Protocol

In the following, we illustrate the main steps of our growing scheme by showing how the MI ground state of this system can be grown. We note that there are more practical ways to prepare the ground state, of course, but the present protocol can be generalized to more complex systems, including states in the FQHE presented in Secs. III and IV.

We will start discussing the protocol in the nondispersive limit $J_2/J_1 \to 0$, where hole excitations will remain localized. The effect of dispersive bands in the case of finite J_1/J_2 will be considered later. Let us assume, that the N particle MI ground state of the SLBHM with filling $\rho = 1/2$ is already prepared in a finite region of the lattice. We now show how the state with $N + 1$ particles can be grown.

1. Topological pump

First, a topological Thouless pump [16,17] is used to create a hole excitation localized at the edge of the system. This process is related to Laughlin's argument of flux insertion [24] in the quantum Hall effect (QHE): Inserting one flux quantum ϕ_0 leads to a quantized particle transport, which is the origin of the quantized Hall conductance σ_{xy}. In the SLBHM, the process of flux insertion is shown in Fig. 2(b). By adiabatically changing the parameters $J_1 - J_2$ and δ in time, we encircle the critical SF region. After a full cycle of period T_ϕ, all particles are shifted one dimer to the right, leaving a hole excitation on the left side of the system. The possibility to construct such a cyclic pump is deeply related to the underlying topology of the model (see Refs. [19,25]).

2. Coherent pump

In the following step, we replenish the hole excitation by a single boson. To this end, we coherently couple a reservoir of particles to the first lattice site of the system as shown in Fig. 3(a). The coherent pump can be described by the Hamiltonian

$$\hat{\mathcal{H}}_\Omega = \Omega \hat{a}_0^\dagger e^{-i\omega t} + \text{H.c.}, \quad (2)$$

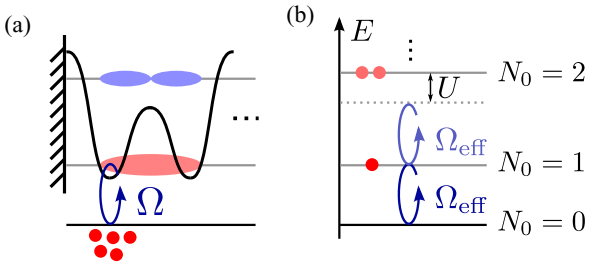

FIG. 3. (Color online) (a) Coherent pump couples a reservoir of bosons to the left-most dimer. (b) Due to a blockade mechanism, only a single particle is pumped into the system. Ω_{eff} is the many-body Rabi frequency, reduced by a Franck-Condon factor, and N_0 is the number of bosons in the left-most dimer.

where Ω is the Rabi and ω the driving frequency. The driving frequency ω is chosen to be resonant with the lowest band. Hence, if $|\Omega|$ is much smaller than the single-particle band gap E_{gap}, particles can only be added in the lowest band. The corresponding Rabi frequency $|\Omega_{\text{eff}}| < |\Omega|$ is then however reduced by a Franck-Condon factor.

In general, the coherent pump (2) creates a coherent superposition state of N_0 bosons in the left-most Wannier orbital of the lowest band. To ensure that, at most, one boson is added, we employ a blockade mechanism, see Fig. 3(b). For sufficiently strong interactions and weak enough driving,

$$U \gg |\Omega_{\text{eff}}| \tag{3}$$

the transition to the $N_0 = 2$ particle state is detuned by the interaction energy U.

For $|\Omega_{\text{eff}}| \ll \Delta$, where Δ is the many-body gap, at maximum one boson can be added into the lowest Bloch band. To replenish the hole excitation by precisely one boson at a time, one can use a π pulse of duration $T_\Omega = \pi/2\Omega_{\text{eff}}$. Although the π pulse is less robust to errors than, e.g., an adiabatic sweep, we choose it because of its speed. This, we believe, is crucial to overcome linear losses present in realistic systems.

Starting from complete vacuum, the sequence described above can be repeated to grow the MI ground state with N particles. Next, we discuss extensions of the protocol, required when the bands are dispersive or the system is finite.

3. *Dispersive bands and finite systems*

Dispersive bands $J_1/J_2 \neq 0$ lead to intrinsic dynamics of the particles and thus of the hole excitations. The bandwidth ΔE of the lowest band sets the time scale for the dispersion. Firstly, the localized quasihole excitation created using the topological pump, disperses into the bulk of the system. Since the coherent pump couples locally to the left-most dimer, the hole cannot be refilled efficiently with a single boson. More importantly, the number fluctuations $\Delta N(t) = [\langle \hat{N}^2 \rangle - \langle \hat{N} \rangle^2]/\langle \hat{N} \rangle$ will increase. To prevent the dynamics of the quasihole excitation, a quasihole trapping potential

$$\hat{\mathcal{H}}_{\text{qh}} = g_{\text{h}}(\hat{a}_0^\dagger \hat{a}_0 + \hat{b}_0^\dagger \hat{b}_0) \tag{4}$$

with strength $g_{\text{h}} > 0$ acting on the left-most dimer can be used. The strength of the trap g_{h} should be weak enough not to destroy the topological phase, but strong enough to trap the quasihole excitation. Concretely we require

$$\Delta E \lesssim g_{\text{h}} \ll \Delta. \tag{5}$$

Secondly, the diffusion of bulk particles from the edge at the right-hand side of the system into vacuum lets the MI melt. Vice versa, the diffusion of holes from the vacuum into the bulk at the right edge of the system makes the state compressible. For fast pump rates of the protocol, this effect can be neglected. However, if the bandwidth ΔE is the dominant contribution, we suggest to use a harmonic trapping potential. The potential should be weak enough to avoid localization effects (see Ref. [26]). Therefore, in local density approximation, the bulk of the system will remain incompressible.

In finite systems with open boundaries, the flux insertion, as illustrated in Fig. 4, connects states from the lower and the upper band at the edges. As long as the upper band is empty, the topological pump creates a hole excitation in the lower band. However, once the boundary on the right-hand side is reached, particles will be excited to the upper band. To avoid the high-energy excitations in the protocol, sufficiently strong losses γ_{Edge} localized at the boundary on the right-hand side of the system can be introduced.

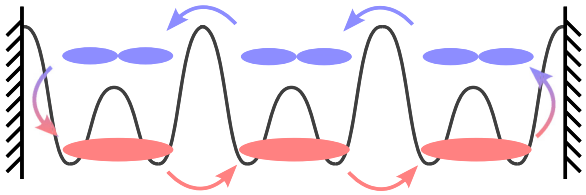

FIG. 4. (Color online) Due to the process of the topological Thouless pump in a finite system, the higher band of the SLBHM will be occupied. While a state at the edge on the right side of the system will be transferred into the upper band, a state from the left upper band, will be transferred to the lower band.

III. FRACTIONAL QUANTUM HALL STATES

We now apply the growing scheme to fractional quantum Hall (FQH) systems. In this case, the bands, i.e., Landau levels (LLs), are nondispersive and we assume an infinite system.

A. Model

We consider a FQH model of bosons in the two-dimensional disk geometry. The magnetic field can be implemented using, e.g., artificial gauge fields. Moreover, we consider a contact interaction between the particles with strength g_0. In second quantized form, the Hamiltonian reads

$$\hat{\mathcal{H}} = \int \mathrm{d}^2\boldsymbol{r}\ \hat{\psi}^\dagger(\boldsymbol{r}) \frac{1}{2M}(\boldsymbol{p} - \boldsymbol{A})^2 \hat{\psi}(\boldsymbol{r}) + \frac{1}{2} g_0 \int \mathrm{d}^2\boldsymbol{r}\ \hat{\psi}^\dagger(\boldsymbol{r}) \hat{\psi}^\dagger(\boldsymbol{r}) \hat{\psi}(\boldsymbol{r}) \hat{\psi}(\boldsymbol{r}), \tag{6}$$

where $\hat{\psi}^\dagger(\boldsymbol{r})$ creates a boson at the position $\boldsymbol{r}$. The first term in Eq. (6) includes the magnetic field in minimal coupling using the vector potential $\boldsymbol{A} = B/2(-y,x,0)$. In this symmetric gauge, the total angular momentum L_z is a conserved quantity, $[\hat{\mathcal{H}}, L_z] = 0$.

For later purposes, we express the field operators $\hat{\psi}(\boldsymbol{r})$ in terms of the bosonic operators $\hat{b}_{n,\ell}$, which create a particle in the orbital of the nth LL with angular momentum ℓ. Here, n and ℓ are integers with $n, \ell + n \geqslant 0$. We obtain

$$\hat{\psi}(\boldsymbol{r}) = \sum_{n,\ell} \eta_{n,\ell}(\boldsymbol{r}) \hat{b}_{n,\ell}, \tag{7}$$

where $\eta_{n,\ell}(\boldsymbol{r})$ are the single-particle wave functions, see, e.g., Refs. [27,28].

B. Laughlin states and excitations: CF picture

It was shown [29–34], that the Laughlin (LN) wave function at magnetic filling $\nu = 1/2$ is the exact zero energy ground state of the bosonic FQH Hamiltonian (6). The filling factor $\nu = N/N_\phi$ is defined as the ratio between the particle number

N and the number of flux quanta N_ϕ. In terms of the complex coordinates $z_j = x_j - iy_j$ of the jth particle, the LN wave function is

$$|\mathrm{LN}, N\rangle \hat{=} \Psi_{\mathrm{LN}} = \mathcal{N}_{\mathrm{LN}} \prod_{j<k} (z_j - z_k)^2 e^{-\sum_j |z_j|^2/4\ell_B^2}, \quad (8)$$

where $\mathcal{N}_{\mathrm{LN}}$ is a normalization constant. The magnetic length $\ell_B = \sqrt{\hbar/B}$ depends on the magnetic field B only.

The zero-energy excitations of the LN wave function are quasiholes described by the wave function $\Psi_{\mathrm{qh}} = \mathcal{N}_{\mathrm{qh}} \prod_j z_j \Psi_{\mathrm{LN}}$. m quasiholes, located in the center, are described by the m quasihole wave function

$$|m\mathrm{qh}, N\rangle \hat{=} \Psi_{m\mathrm{qh}} = \mathcal{N}_{m\mathrm{qh}} \left(\prod_j z_j \right)^m \Psi_{\mathrm{LN}}. \quad (9)$$

The LN state $|\mathrm{LN}, N\rangle$ and the quasihole state $|m\mathrm{qh}, N\rangle$ carry different total angular momentum L_z,

$$L_z(|\mathrm{LN}, N\rangle) = N(N-1), \quad (10)$$

$$L_z(|m\mathrm{qh}, N\rangle) = N(N-1) + mN. \quad (11)$$

Both wave functions can be understood in the more general framework of composite fermions (CFs) [28,36–38]. For the $\nu = 1/2$ case, the LN wave function (8) can be decomposed into

$$\Psi_{\mathrm{LN}} = \mathcal{N}_{\mathrm{LN}} \prod_{j<k} (z_j - z_k) \Phi_{\mathrm{CF}}^{(\nu^*=1)}. \quad (12)$$

Besides the Jastrow factor $\prod_{j<k}(z_j - z_k)$ attaching one flux quantum to each boson [see Fig. 5(b)], a fermionic wave function $\Phi_{\mathrm{CF}}^{(\nu^*=1)}$ appears. The Jastrow factor screens the interactions between the particles and leads to a reduced magnetic field $B^* = B/2$ seen by the CFs. As in the IQHE, their wave function is given by a Slater determinant of single-particle orbitals filling the lowest CF-LL $\nu^* = 1$, i.e., $\Phi_{\mathrm{CF}}^{(\nu^*=1)} = \prod_{j<k}(z_j - z_k) \exp(-\sum_j |z_j|^2/4\ell_B^2)$.

The FQHE can be interpreted as an IQHE of noninteracting CFs in a reduced magnetic field B^*. The CF picture in the context of the FQHE is powerful in describing all fractions in the Jain sequence [38] and moreover describes the quasihole excitations and their counting correctly. However, naive replacement of the magnetic field B with the effective magnetic field B^* in the cyclotron frequency $\omega_c = B/M$ does not reproduce the correct Laughlin gap Δ_{LN}. Here, a microscopic theory of the full interacting many-body problem is necessary. The wave functions constructed from the CF theory provide a good variational ansatz to calculate the energy of the ground state and its excitations [28]. Moreover, in order to explain fractions not included in the Jain sequence of FQH states, interactions between CFs need to be taken into account.

C. Protocol

1. Topological pump: flux insertion

In the toy model II A, we used a topological Thouless pump to shift the particles to the right. In the context of quantum Hall physics, this corresponds to Laughlin's argument of flux insertion [24], which was used to explain the quantization of the Hall conductivity. The idea is to insert locally in the center of the system flux quanta ϕ_0 in time T_ϕ, which produces an outwards Hall current $j_r \sim \mathrm{Ch}\ \partial_t \phi$ in radial direction. The quantization of the Hall current is related to the nontrivial Chern number Ch of the system. The process of inserting flux quanta increases the total angular momentum of the state. A more detailed discussion of the process in the noninteracting case can be found in Appendix A.

Starting from the $\nu = 1/2$ LN state $|\mathrm{LN}, N\rangle$ with N particles, we insert two flux quanta $2 \times \phi_0$ in time T_ϕ in the center of the system. In this way, we create a two-quasihole excitation $|2\mathrm{qh}, N\rangle$. The two-quasihole state $|2\mathrm{qh}, N\rangle$ already

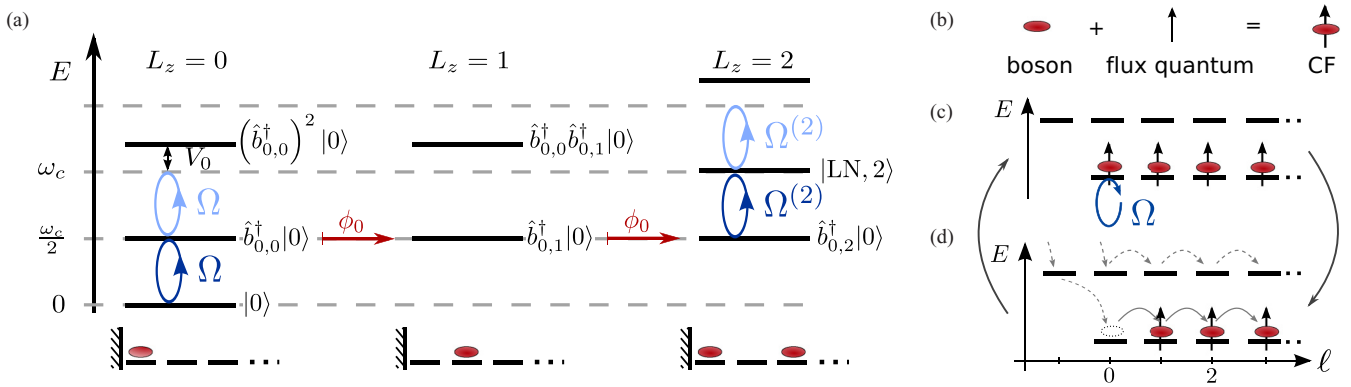

FIG. 5. (Color online) (a) Growing scheme for the $\nu = 1/2$ LN state in the continuum. The many-body eigenstates of the FQH Hamiltonian (6), between which transitions are driven, are shown as a function of the total conserved angular momentum L_z. Starting from the vacuum $|0\rangle$, the LN state with $N = 2$ bosons is grown. After adding one boson in the central orbital, two flux quanta are adiabatically inserted and the resulting hole excitation is refilled by a second boson. This can be interpreted as replenishment of the system by a composite fermion, hence keeping intact the topological order of the system. The lowest line shows the schematics of the prepared states after every step. (Horizontal lines denote orbitals; this picture is valid in the thin-torus limit or after using the patterns as partitions determining certain Jack polynomials [35].) (b) Flux attachment: a single boson together with one flux quantum form a CF. (c) and (d) Level spectrum in terms of CFs. (c) Coherent pump process with Rabi frequency Ω. The lowest CF-LL is filled, corresponding to CF filling factor $\nu^* = 1$. (d) Flux insertion process increases angular momentum ℓ by one.

lies in the same angular momentum L_z sector as the LN state $|\mathrm{LN}, N+1\rangle$ with $N+1$ particles [compare Eqs. (10) and (11)].

2. Coherent pump

In the next step, we refill the quasihole excitation using a coherent pump, which couples a reservoir of bosons to the hole excitation. As this is done in the center, no angular momentum is transferred. To this end, we supplement the FQH Hamiltonian (6) by a term

$$\hat{\mathcal{H}}_\Omega = \int \mathrm{d}^2\boldsymbol{r}\; g(t)\mathrm{e}^{-i\omega t}\delta^2(\boldsymbol{r})\hat{\psi}^\dagger(\boldsymbol{r}) + \mathrm{H.c.} \tag{13}$$

While $g(t)$ denotes the strength of the coherent pump, the driving frequency $\omega = \omega_c/2$ is chosen resonant with the lowest LL (LLL). In the regime of large magnetic fields and low temperatures, it is sufficient to project Eq. (13) to the LLL resulting in

$$\hat{\mathcal{P}}_{\mathrm{LLL}}\hat{\mathcal{H}}_\Omega\hat{\mathcal{P}}_{\mathrm{LLL}} = \Omega\mathrm{e}^{-i\omega t}\hat{b}^\dagger_{0,0} + \mathrm{H.c.}, \tag{14}$$

where we defined the Rabi frequency $\Omega = g/\sqrt{2\pi\ell_\mathrm{B}^2}$. This corresponds to Ω_{eff} in the toy model.

Since the coherent pump does not change the angular momentum L_z sector, we obtain a similar blockade mechanism as in the toy model [see Fig. 5(a) with $L_z = 0,2$]. In the corresponding sector, there is only one zero-interaction energy eigenstate, the $N+1$ LN state. The energy offset to any other states in the $(N+1)$-particle manifold is of the order of Haldane's zeroth pseudopotential V_0 [39]. We require $\Omega \ll \omega_c, V_0$ to avoid excitations to high energy states.

To insert a single particle, we use a π pulse of duration $T_\Omega = \pi/2\Omega^{(N)}$. Here, the bare Rabi frequency Ω is reduced by a Franck-Condon factor

$$\Omega^{(N)}/\Omega = \langle \mathrm{LN}, N|\hat{b}^\dagger_{0,0}|2\mathrm{qh}, N-1\rangle, \tag{15}$$

which accounts for the overlap between the initial and final state. In Fig. 6, we show the Franck-Condon factors for different particle number N and extrapolate to $N \to \infty$. To this end, we calculated the LN wave function using exact diagonalization.[1] A linear fit suggests that even in the case $N \to \infty$ the Franck-Condon factor does not vanish with $\Omega^{(\infty)}/\Omega \simeq 0.7$.

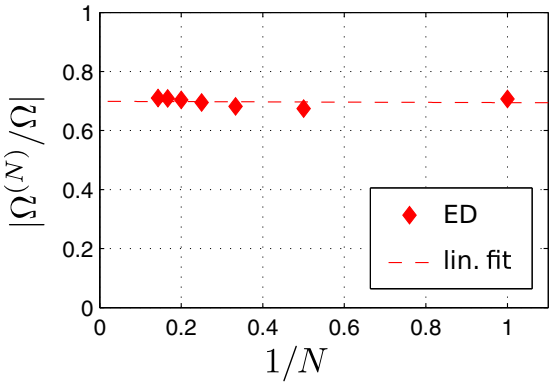

FIG. 6. (Color online) Franck-Condon factors $\Omega^{(N)}/\Omega$, as defined in Eq. (15), for different particle numbers N calculated using exact diagonalization (ED) in a system with contact interaction for up to $N = 7$ particles. A linear fit is used to extrapolate $N \to \infty$.

3. CF picture

The first few steps of the protocol are illustrated in Fig. 5(a). Another description of the protocol, which provides a much simpler physical picture uses the CF picture. Firstly, due to local flux insertion [see Fig. 5(d)], we generate a quasihole excitation. Secondly, the hole excitation is refilled by an effective coherent CF pump, for a particle together with one flux quantum. Analogously to the blockade mechanism, one CF refills the empty $\ell = 0$ orbital [see Fig. 5(c)]. By subsequent repetition, we grow the filling $\nu^* = 1$ integer quantum Hall state of noninteracting CFs in a reduced magnetic field B^*.

The CF picture provides an explanation, why it is possible to grow highly correlated LN states. Since the CF wave function $\Phi_{\mathrm{CF}}^{(\nu^*=1)}$ is a separable Slater determinant of noninteracting CFs, we can grow the highly correlated LN state by adding CFs one by one to the system. Note that, although the wave function is a separable product state of CFs occupying Wannier functions (or Landau level orbitals), it has nonlocal topological order. This is because Wannier functions (or orbitals) of a single LL are nonlocal [40]. On first glance, this may look contradicting as the dynamical growing scheme presented in this paper involves only local processes. However, the nonlocal topological order in the system is generated by the Thouless pump (flux insertion).

D. Performance

For interesting applications such as measuring the braiding statistics of elementary excitations, the LN state has to be prepared with high accuracy. To quantify the quality of the scheme, we calculate the fidelity $\mathcal{F}_N$ of being in the LN state with N particles after N steps of the protocol. The fidelity is defined as

$$\mathcal{F}_N = |\langle\Psi_N|\mathrm{LN}, N\rangle|, \tag{16}$$

where $|\Psi_N\rangle$ is the state after N steps of the protocol. In the calculation of the fidelity $\mathcal{F}_N$ we include besides nonadiabatic transitions in the flux insertion and coherent pump process, a particle loss rate γ. This is important, since decay usually plays a crucial role, in particular in photonic systems.

The total time for a full cycle (flux insertion time T_ϕ, coherent pump time T_Ω) is $T = T_\phi + T_\Omega$. As will be discussed in detail later, we find for the fidelity perturbatively in the limit $\gamma T, (\Delta_{\mathrm{LN}}T_\phi)^{-1}, (\Delta_{\mathrm{LN}}T_\Omega)^{-1} \ll 1$

$$\mathcal{F}_N \simeq \exp\left[-\frac{1}{2}N\left(\frac{1}{2}\gamma T(N+1) + \frac{\Lambda_N^2}{(\Delta_{\mathrm{LN}}T)^2}\right)\right], \tag{17}$$

where Λ_N depends weakly on N and will be seen later to converge to a finite value for large N. We see that the losses

[1] Exact diagonalization is used to obtain the coefficients of the monomials $z_1^{m1}\ldots z_N^{m_N}$ in the Laughlin state represented in the angular momentum basis. Another approach would be to use Jack polynomials [35].

and the nonadiabatic transitions contribute competitively in Eq. (17). While it is favorable to run the protocol as fast as possible to avoid losses, the adiabaticity requires long time scales T.

For fixed fidelity $\mathcal{F}_N = 1-\varepsilon$, $\varepsilon \ll 1$, we calculate the maximal number of particles $N_{\max}$ which can be grown with optimal period $T_{\rm opt}$ using the asymptotic value of $\Lambda_N \to \Lambda$ for $N \to \infty$. To leading order in N, we approximately obtain

$$N_{\max} \simeq 1.365\varepsilon^{3/5}\left(\frac{\Delta_{\rm LN}}{\Lambda\gamma}\right)^{2/5}, \tag{18}$$

$$T_{\rm opt} \simeq 1.431\,(\varepsilon\gamma)^{-1/5}\left(\frac{\Lambda}{\Delta_{\rm LN}}\right)^{4/5}. \tag{19}$$

The LN state with fildelity $\mathcal{F}_N = 1-\varepsilon$ can be grown in time $T_0 = N_{\max}T_{\rm opt} \sim N_{\max}^{3/2}\varepsilon^{-1/2}\Lambda/\Delta_{\rm LN}$ scaling only slightly faster than linear with particle number $N_{\max}$. Note that the fidelity decreases with increasing time $t > T_0$. In the following, we discuss the different contributions to the fidelity (17) in detail. In particular, we find three major error sources related to losses, flux insertion and coherent pump, which yields

$$\mathcal{F}_N = \exp\big(-\tfrac{1}{2}(P_\gamma + NP_\phi + NP_\Omega)\big). \tag{20}$$

1. Loss

We assume a particle loss rate $\gamma \ll 1/T$, i.e., after one full period T, the probability of loosing a particle is small. The probability of a single decay process after N steps of the protocol is then given by

$$P_\gamma = 1-\exp\left(-\gamma T\sum_{n=1}^{N} n\right) \simeq \frac{1}{2}\gamma T N(N+1). \tag{21}$$

To leading order in N, the probability of loosing one particle increases quadratically with the particle number N.

2. Flux insertion

The process of flux insertion, as described in Sec. III C, introduces one flux quantum ϕ_0 in the center of the system. For simplicity, we assume the flux $\phi(t) = \phi_0\, t/T_\phi$ to change linearly in time t. In the fully adiabatic protocol, the angular momentum ℓ is therefore increased by one without coupling different LLs n,n'. We calculate in the noninteracting case the nonadiabatic coupling matrix element $\kappa = \langle n',\ell|-i\,\partial_\ell|n,\ell\rangle$ between different LLs. To estimate the scaling of the probability P_ϕ for excitation of higher LLs, we consider the coupling between the LLs n and $n+1$. In the regime of long times T_ϕ, we determine P_ϕ perturbatively (see Appendix B). Using the Laughlin gap $\Delta_{\rm LN}$, we obtain

$$P_\phi \simeq \frac{\bar\kappa^2}{(\Delta_{\rm LN}T_\phi)^2}, \tag{22}$$

where $\bar\kappa \simeq 1$ is a nonuniversal coupling constant. Importantly, nonadiabatic transitions to higher LLs scale as $\sim 1/(\Delta_{\rm LN}T_\phi)^2$.

3. Coherent pump

The coherent pump (14), as discussed in III C, couples in zeroth order in $\Omega/\Delta_{\rm LN}$ only the two-quasihole state $|2{\rm qh},N\rangle$ to the Laughlin state $|{\rm LN},N+1\rangle$. In first-order perturbation theory, couplings to excited states in the $N-1,N,N+1$, $N+2$ particle sectors are relevant. We obtain for the probability of nonadiabatic excitations,

$$P_\Omega \simeq \frac{\sigma_N^2}{(\Delta_{\rm LN}T_\Omega)^2}, \tag{23}$$

where we used the π-pulse time $T_\Omega = \pi/2\Omega$. The nonuniversal factor σ_N includes Franck-Condon factors and excitation energies $\Delta^{(N)}$ of undesired states weighted by the Laughlin gap $\Delta_{\rm LN}$ (see Appendix C). In Fig. 7, σ_N is calculated for various particle numbers N using exact diagonalization. For $N \to \infty$, we extrapolate with a quadratic fit $\sigma_\infty \simeq 1.4$.

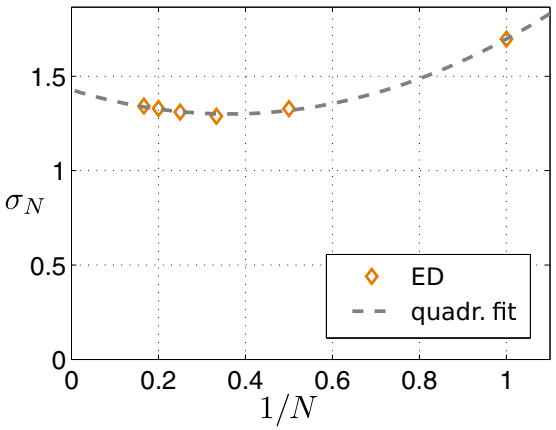

FIG. 7. (Color online) Scaling of the nonuniversal factor σ_N from Eq. (23) with particle number N. We interpolate $N \to \infty$ with a quadratic fit.

When putting together expressions (21)–(23), we obtain Eq. (17) for fixed ratio T_Ω/T_ϕ, where the factor Λ_N is defined as

$$\Lambda_N^2 = \bar\kappa^2(T/T_\phi)^2 + \sigma_N^2(T/T_\Omega)^2. \tag{24}$$

To estimate the value of Λ_N, we use values for $\bar\kappa,\sigma_N$ obtained from the asymptotic limit $N \to \infty$ in our numerical calculations. For a typical ratio $T_\Omega/T_\phi = 6$ later on used in the numerical simulations for the lattice case, we find $\Lambda \simeq 7$.

IV. LATTICE AND FRACTIONAL CHERN INSULATORS

Lattice systems are promising candidates to realize FQH physics, since the magnetic fields realized in these systems are very strong, such that low magnetic filling factors $\nu \leqslant 1$ can be achieved while keeping a sufficiently large density of particles. However, in this case, the magnetic length $\ell_{\rm B}$ and the lattice constant a become of comparable size. Therefore lattice effects, such as dispersive bands, play a crucial role. Now, we introduce an effective CF lattice model, which allows us to include these effects in our investigation. Moreover, we consider finite systems now, where edge states are present.

A. Hofstadter Hubbard model

We consider a two-dimensional lattice described in a tight-binding model with nearest-neighbor hopping terms J. The Peierls phases are chosen to mimic a magnetic field in

Landau gauge. Additionally, we consider on-site interactions U resulting in the following Hofstadter Hubbard Hamiltonian:

$$\hat{\mathcal{H}} = -J\sum_{x,y}(\hat{a}^\dagger_{x+1,y}\hat{a}_{x,y}e^{-i2\pi\alpha y} + \hat{a}^\dagger_{x,y+1}\hat{a}_{x,y} + \text{H.c.}) + U/2\sum_{x,y}\hat{a}^\dagger_{x,y}\hat{a}^\dagger_{x,y}\hat{a}_{x,y}\hat{a}_{x,y}. \quad (25)$$

The x,y coordinates are measured in units of the lattice constant a. We use the operators $\hat{a}_{x,y}$ to denote the bosonic annihilation of a particle at site (x,y). The flux per plaquette α (in units of the flux quantum) accounts for the magnetic field penetrating the two-dimensional lattice. In particular, it sets the magnetic length $\ell_B = a/\sqrt{2\pi\alpha}$, which describes the extent of the cyclotron orbits.

In recent experiments, the Hofstadter model was realized in a photonic system [11] as well as in ultracold gases [7,8]. The photonic system [11] implements a tight-binding model using ring resonators in the optical wavelength regime. The tunneling is achieved using off-resonant ring resonators, which have a different length for hopping forward and backward and the Peierls phases are determined by the optical path difference. As explained in Ref. [41], the local change of the optical path difference, e.g., by heating elements, allows to realize Laughlin's gedankenexperiment of flux insertion. In experiments with ultracold gases [7,8], standing waves are used to create a two-dimensional optical lattice. Due to a strong field gradient along one direction, the particles are localized. Using laser-assisted tunneling techniques, the hopping elements are implemented with an additional Peierls phase. In the experiments, the Peierls phase can be engineered to realize, e.g., a flux per plaquette of $\alpha = 1/4$. Introducing flux quanta locally into the system requires control over individual Peierls phases, which seems to be quite challenging in these systems. In the continuum, it may be feasible to create a quasihole excitation by adiabatically increasing the intensity of a tightly focused laser beam [42] or using an orbital angular momentum beam to insert the right amount of angular momentum into the system [43,44]. Note that the continuum limit $\alpha \to 0$, where the magnetic length ℓ_B is much larger than the lattice constant a, corresponds to the FQH model (6).

B. Ground state and excitations

We summarize the properties of the ground state of the Hofstadter Hubbard model (25) for bosons with magnetic filling factor $\nu = 1/2$ in two different geometries. In the case of a *torus* discussed in Refs. [45,46], the exact ground state was compared to the Laughlin state (8) projected on a lattice for different flux per plaquette α. It was found, that the Laughlin wave function provides a good description up to $\alpha \simeq 0.2$. Moreover, the many-body Chern number remains $\text{Ch} = 1/2$ until the flux per plaquette reaches a critical value of $\alpha \simeq 0.4$. The size of the Laughlin gap Δ_{LN} depends on the parameters α and U. For instance, at $\alpha \simeq 0.1$, the Laughlin gap saturates at $\Delta_{LN} \simeq 0.1J$ for large $U \gg J$.

In Ref. [15], we numerically analyzed the ground state in a spherical geometry using a buckyball lattice with $N_s = 60$ sites [see Fig. 8(a)]. To realize a filling $\nu = 1/2$ in the continuum on a sphere, the relation between particle number N and flux quanta N_ϕ is $N_\phi = 2(N-1)$. We identify the topological order of the ground state by inserting two flux quanta ϕ_0 in a system with $N = 3$ particles and $N_\phi = 4$ flux quanta. The many-body spectrum E_ϕ during flux insertion is shown in Fig. 8(b). We observe a single incompressible ground state with a many-body gap $\Delta \simeq 0.1J$ for $U = 10J$, similar to the case on a torus. Importantly, we obtain the correct counting of nearly degenerate quasihole states after inserting one and two flux quanta as expected from the continuum limit on a sphere. In both lattice cases, we expect the ground state to be in the same topological universality class as the LN state in the continuum.

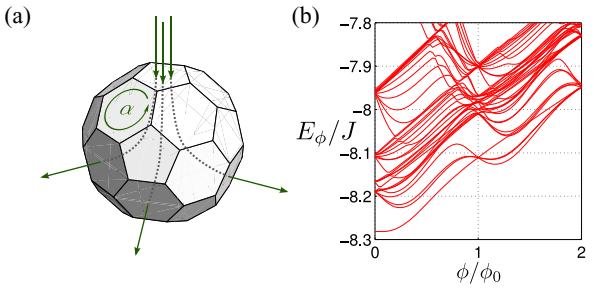

FIG. 8. (Color online) (a) Flux insertion on a C_{60} buckyball geometry. (b) Many-body spectrum $E(\phi)$ on a C_{60} buckyball starting with $N = 3$ particles and $N_\phi = 4$ flux quanta and introducing two more flux quanta $2 \times \phi_0$ with $U = 10J$.

C. Effective CF lattice model

Before we introduce the effective CF lattice model, we briefly summarize the results of the exact simulations in Ref. [15]. We implemented the protocol on a C_{60} lattice up to $N = 3$ particles with $U = 10J$. Additionally, we used a similar quasihole trapping potential as in Eq. (4). The numerical results show, that the state $|\Psi(t)\rangle$ prepared after three steps of the protocol is close to the LN ground state $|\text{gs}\rangle$ with $N = 3$ particles. Moreover, as expected from the blockade mechanism in the coherent pump, the number fluctuations $\Delta N(t)$ are small throughout the protocol.

To discuss edge effects, larger systems with many particles are required, such that bulk and edge states can be distinguished. However, using exact diagonalization, only a few particles are feasible on large lattice systems with $N_s \gtrsim 60$ sites. To simulate such a system, we need an effective model describing the low-energy dynamics of the Hamiltonian (25).

In the spirit of the composite fermion principle, we assume a model of noninteracting composite fermions on a lattice. By attaching one flux quantum to a boson, as shown in Fig. 5(b), an (approximately) noninteracting composite fermion is formed in a reduced magnetic field. The simplest tight-binding model with a reduced magnetic field, $\alpha^* = \alpha/2$, only considers nearest-neighbor hopping elements J^*. Under these assumptions, the effective model is

$$\hat{\mathcal{H}}_{CF} = -J^*\sum_{x,y}(\hat{c}^\dagger_{x+1,y}\hat{c}_{x,y}e^{-i2\pi\alpha^* y} + \hat{c}^\dagger_{x,y+1}\hat{c}_{x,y} + \text{H.c.}), \quad (26)$$

where $\hat{c}^\dagger_{x,y}$ creates a composite fermion at site (x,y). The only free parameter J^* in this model determines the time scale of the

dynamics. By comparing the bandwidth of the full many-body spectrum of interacting bosons to the free CF single-particle spectrum on a C_{60} buckyball at $N_\phi = 6$ flux quanta, we find $J^* \simeq J$.

Now, we conjecture that the effective CF lattice model describes correctly the low-energy dynamics. Yet, there is no proof that the CF theory is applicable in a lattice. However, there are several hints that the essential physics can still be understood in terms of CFs. First of all, the CF picture in a lattice captures the correct counting of quasihole excitations.[2] Thus the low-energy excitations should be described correctly. Moreover, the LN wave function is a special case of the more general CF theory, when the lowest CF-LL $n^* = 0$ is filled. As shown in Ref. [45], the LN wave function projected on a lattice describes the many-body ground state on a lattice accurately up to relatively high flux per plaquette $\alpha \simeq 0.2$. Therefore we limit the flux per plaquette in our effective model to $\alpha^* \leqslant 0.1$. Finally, CF states from the Jain sequence [38], other than the LN state, have been identified in a lattice [47,48] for small flux per plaquette. Therefore we expect that this effective model captures the essential physics of the original many-body model in the lowest Chern band (LChB), including the dynamics of the hole excitations. As this model is supposed to describe only the low-energy regime, excitations to higher Chern bands (HChBs) are not expected to be described correctly.

D. Numerical results

1. Numerical implementation of the protocol

The protocol is implemented in both, the spherical geometry on a C_{60} buckyball as in Ref. [15] as well as the square lattice with open boundary conditions. We use the method explained in Ref. [15] to insert flux quanta locally.

Unlike the coherent boson pump (13), we model the coherent CF pump by coupling a CF reservoir mode to the central site of the system. The reservoir mode is refilled in each step of the protocol. Therefore we insert at most one CF per cycle. This is similar to the blockade mechanism for bosons and therefore only justified in the limit of large interactions $U \gg J$, where corrections scale as $(\Omega/\Delta_{\mathrm{LN}})^2$ [see Eq. (23)]. Moreover, we implement the quasihole trapping potential by including an on-site potential g_{h} on the central site.

As explained for the toy model, in the case of a finite square lattice we introduce loss channels at the boundaries of the system to prevent high energy excitations. Then, we calculate the time evolution of the correlation matrix elements $\langle \hat{c}^\dagger_{x,y} \hat{c}_{x',y'} \rangle$ by solving the corresponding master equation in Lindblad form ($\hbar = 1$),

$$\partial_t \hat{\rho} = -i[\hat{\mathcal{H}}_{\mathrm{CF}}, \hat{\rho}] + \frac{1}{2} \sum_{x,y}{}' 2\hat{l}_{x,y} \hat{\rho} \hat{l}^\dagger_{x,y} - \{\hat{l}^\dagger_{x,y} l_{x,y}, \hat{\rho}\}, \quad (27)$$

numerically. Absorbing boundary conditions are described by the jump operators $l_{x,y} = \sqrt{\gamma_{\mathrm{Edge}}} \hat{c}_{x,y}$ with loss rate γ_{Edge} and we restrict the sum $\sum'$ to the edge of the system.

[2]Note that the counting of quasihole excitations on a C_{60} buckyball lattice and the counting in the continuum on the sphere are equal and thus also the CF counting is correct.

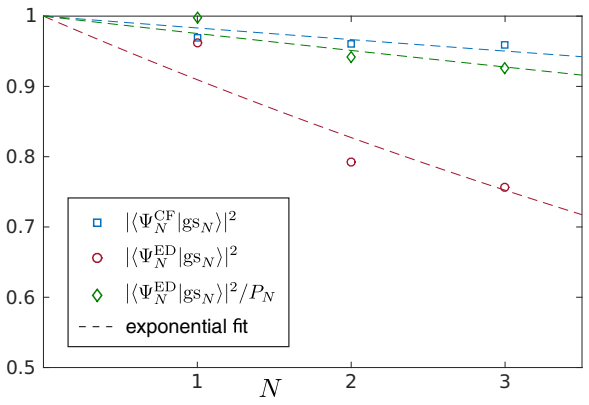

FIG. 9. (Color online) Comparison of ED result from Ref. [15] (red circles) with the result obtained using the effective CF model (blue squares) on a C_{60} buckyball. Also shown are the ED results after projecting to the correct particle number sector (green diamonds). The parameters are $U = 10J$, $g_{\mathrm{h}} = J$, $\Omega = 0.05J$. We adjust the π-pulse time $T_\Omega \simeq 6\pi/\Omega$ to obtain the maximal particle number N in each step. The time for flux insertion is $T_\phi = 20\pi/J$. The dashed lines indicate an exponential fit for the fidelity $\mathcal{F}_N^2$ [see Eq. (17) with $\gamma = 0$].

Note that the loss of a CF is a loss of both, a flux quantum and the boson it was attached to. Therefore we only allow this loss term at the edge of the system, where the meaning of a free flux quantum without a particle is obsolete.

2. Comparison: effective CF model with ED

For small particle numbers N, we compare the results of the protocol in Ref. [15] using exact diagonalization (ED) with the effective CF description introduced here. The comparison is shown in Fig. 9, where we plot the overlaps squared $|\langle\Psi_N^{\mathrm{ED}}|\mathrm{gs}_N\rangle|^2$ (ED) and $|\langle\Psi_N^{\mathrm{CF}}|\mathrm{gs}_N\rangle|^2$ (CF model) for up to three steps. We use an exponential fit to estimate the values of Λ for the scaling of the fidelity [see Eq. (17)]. For the ED result we obtain $\Lambda_{\mathrm{ED}} \simeq 13$, while $\Lambda_{\mathrm{CF}} \simeq 5$ in the effective CF model.

We attribute the discrepancy between the two results to the following reasons: (i) In the CF model at most one particle can be inserted into the system due to Pauli blocking. In contrast, the ED simulation of Ref. [15] suggests a non-negligable contribution to the infidelity due to occupation of higher particle number sectors (see discussion in Appendix C). From Eq. (23), we find, using our numerical data, that the error scales as $(\Omega/\Delta_{\mathrm{LN}})^2 \simeq 0.25$. Indeed, projecting the ED result to the correct particle number sector, $|\langle\Psi_N^{\mathrm{ED}}|\mathrm{gs}_N\rangle|^2/P_N$, as done also in Fig. 9, gives much better agreement with the CF description. (ii) To grow the LN state at filling $\nu = 1/2$, we introduce two flux quanta into the system in every step, with corrections scaling as in Eq. (22). In the effective CF description on the other hand, only one flux quantum is inserted into the system per step. The second flux quantum can be thought of being attached to the CF that is added afterwards. Hence the flux insertion contribution to the infidelity is slightly larger in the ED simulation than in the CF model.

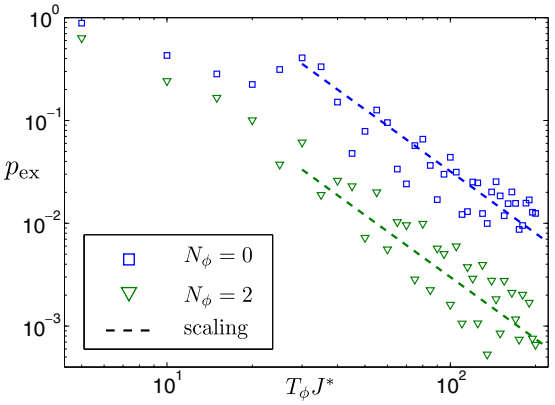

FIG. 10. (Color online) Shown is the excitation probability $p_{\rm ex}$ to high-energy states in the case of flux insertion. Starting with particle number $N = 1$ ($N = 3$) in the ground state $|{\rm gs}\rangle$ at $N_\phi = 0$ ($N_\phi = 2$) flux quanta, we insert one flux quantum and analyze the probability $p_{\rm ex}$ of being in an excited state for various flux insertion times T_ϕ. The dashed lines indicate the expected scaling from Eq. (22) in Sec. III D.

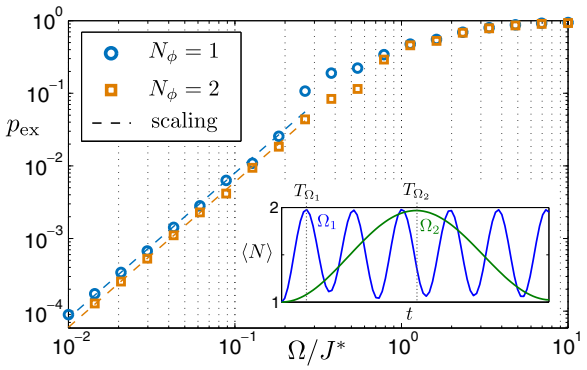

FIG. 11. (Color online) We show the excitation probability $p_{\rm ex}$ to high energy states for different Rabi frequencies Ω in the coherent CF pump. Starting from the quasihole state with $N_\phi = 1$ ($N_\phi = 2$) flux quantum, we coherently couple to the ground state with $N = 2$ ($N = 3$) particles for various Rabi frequencies Ω. The dashed lines indicate the expected scaling from Sec. III D. In the inset, we extract the π-pulse time T_Ω when the maximal number of particles is in the system, for two different values of Ω.

3. Performance

To investigate the performance of the protocol, we use the spherical geometry without edges. The bandwidth $\Delta E/J$ of the C_{60} buckyball with up to $N_\phi = 6$ flux quanta is small and thus we can neglect the effect of dispersive bands. In Sec. III D, we have seen that the topological pump as well as the coherent pump in the continuum need sufficiently long times $T_\phi, T_\Omega \gg \Delta_{\rm LN}^{-1}$ to avoid nonadiabatic excitations. The excitation probability to the excitonic states scale as $P_\phi \sim T_\phi^{-2}$, $P_\Omega \sim T_\Omega^{-2} \sim \Omega^2$ [see Eqs. (22) and (23)]. Here, we show that the scaling for P_ϕ, P_Ω also holds for the lattice in the perturbative regime.

Firstly, we analyze the excitation probability $p_{\rm ex}$ in the case of *flux insertion*. We start from the ground state $|{\rm gs}\rangle$ with $N = 1$ ($N = 3$) particle(s) at $N_\phi = 0$ ($N_\phi = 2$) flux quanta and insert one flux quantum in time T_ϕ to create a CF quasihole excitation $|{\rm qh}\rangle$. Figure 10 shows the probability $p_{\rm ex}$ for excitation of higher bands. Besides an oscillatory behavior with increasing duration T_ϕ, we confirm the expected scaling $P_\phi \sim T_\phi^{-2}$in the perturbative regime.

To analyze the excitation probability $p_{\rm ex}$ for the *coherent CF pump*, we start from the quasihole state $|{\rm qh}\rangle$ at $N_\phi = 1$ ($N_\phi = 2$) flux quantum. The coherent pump is coupled resonantly to the hole excitation for different bare Rabi frequencies Ω. In Fig. 11, we plot $p_{\rm ex}$ for different Ω. The time T_Ω needed for a π pulse is determined by the maximal achievable particle number $\langle N \rangle$ (see inset Fig. 11). For time T_Ω, we extract the excitation probability $p_{\rm ex}$ of being not in the ground state with $N = 2$ ($N = 3$) particles. We find excellent agreement with the expected scaling in the perturbative regime.

4. Dispersive bands: quasihole trapping

As noted in the toy model Sec. II, the finite bandwidth leads to an intrinsic dispersion of the quasihole excitations. Without trapping the hole excitations, the coherent pump cannot replenish them efficiently.

We numerically analyze the effect of dispersive bands on a square lattice. The results are shown in Fig. 12, where we compare the number of CFs $\langle N \rangle(t)$ for 25 cycles of the protocol with and without quasihole trapping potential $g_{\rm h}$. Here, $T = T_\phi + T_\Omega$ is the time needed for one step of the protocol. The trapping potential improves the efficiency of the growing scheme already after three steps. Therefore we include the quasihole trapping potential $g_{\rm h}$ for the following discussions.

5. Finite systems: edge decay

Let us finally discuss the effects of a finite system, where edge states are present. In particular, we are interested in the case $L/\ell_{\rm B} \ll T\gamma$, where L is the linear system size. In this case, particles reach the boundary of the system before they decay. Hence, edge states become important in this regime. As explained in the toy model Sec. II, during the protocol edge states will transport particles to high energy states. Below we will argue that, to reach integer filling in the

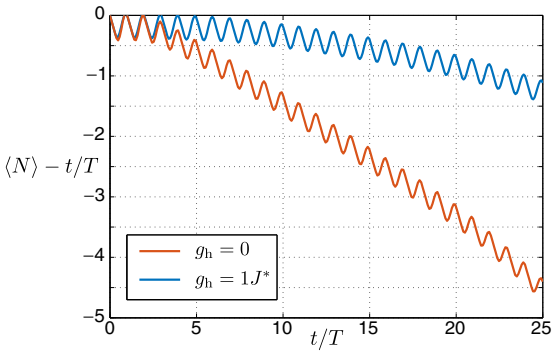

FIG. 12. (Color online) Shown is the number of particles $\langle N \rangle$ during the protocol in time t/T in a system with and without trapping potential $g_{\rm h}$. The lattice size is 11×11 with an effective flux per plaquette $\alpha^* = 0.1$. We insert flux in time $T_\phi = 60/J^*$. The π-pulse time T_Ω for $g_{\rm h} = 0$ ($g_{\rm h} = 1J^*$) is $T_\Omega = 100/J^*$ ($T_\Omega = 130/J^*$).

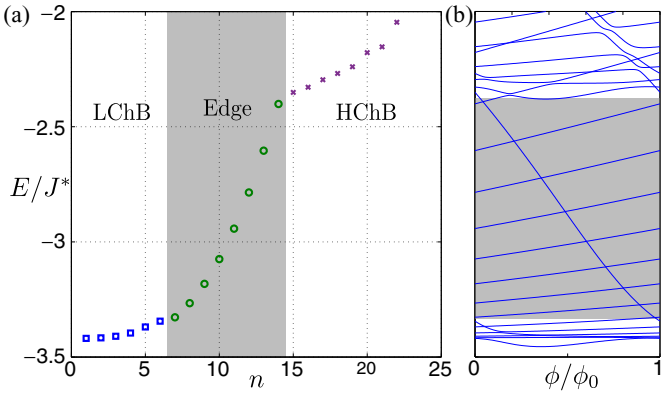

FIG. 13. (Color online) (a) Low-energy spectrum of the CF Hamiltonian (26) with $\alpha^* = 0.1$ and lattice size 11×11. States are labeled with number n. We identify three different sectors using additionally the density distribution of the states: lowest Chern band (LChB) $n = 1, \ldots, 6$, edge states (Edge) $n = 7, \ldots, 14$ and higher Chern bands (HChBs) $n \geqslant 15$. (b) Energy spectrum during insertion of one flux quantum ϕ_0 with parameters as in (a).

LChB, absorbing boundaries can be implemented to prevent excitations to HChBs.

In the case of open boundary conditions, we identify three different regimes in the single-particle spectrum of the CFs, shown in Fig. 13(a). Due to the finite size of the system, edge states occur between the states of the LChB and those of the HChB. Crucially, the effective CF model on the lattice is not supposed to describe the dynamics of the high-energy states correctly. To prepare a LN type state in the bulk of a finite system, it is necessary to avoid high energy excitations.

The free CF energy spectrum of a finite system with trapping potential g_h during adiabatic flux insertion is depicted in Fig. 13(b). Besides the creation of a hole excitation in the LChB, edge states occur connecting the low- and high-energy states. Due to the edge states, particles will be excited to the HChBs of the system during the protocol.

This is shown in Fig. 14, where we analyze the particle number $\langle N_{\mathrm{LChB}}\rangle, \langle N_{\mathrm{Edge}}\rangle, \langle N_{\mathrm{HChB}}\rangle$ in the three different

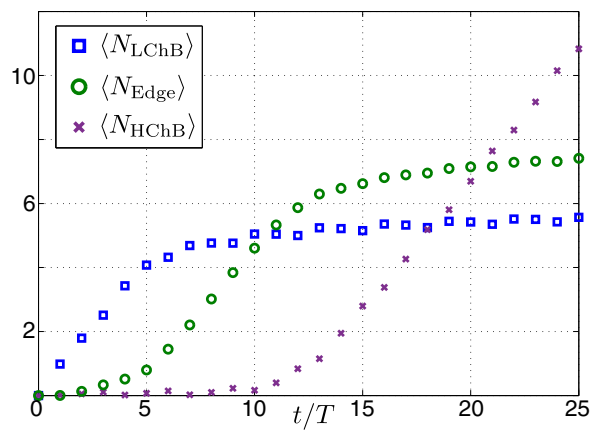

FIG. 14. (Color online) Particle number $\langle N_{\mathrm{LChB}}\rangle$, $\langle N_{\mathrm{Edge}}\rangle$, $\langle N_{\mathrm{HChB}}\rangle$ in the three different energy sectors, defined in Fig. 13(a), after each cycle in the protocol. The parameters used here are the same as in Fig. 12 with trapping potential g_h.

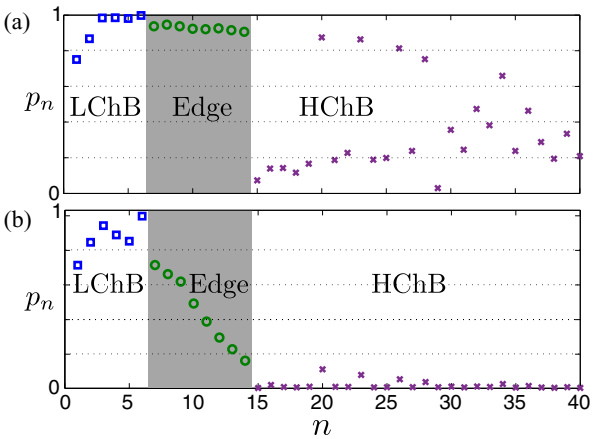

FIG. 15. (Color online) Population p_n of the low-energy CF states at the end of the protocol. (a) Parameters as in Fig. 12 after 25 steps of the protocol and (b) after 35 steps of the protocol with absorbing boundary conditions ($\gamma_{\mathrm{Edge}} = 0.0025J^*$). Note, the coherent pump couples mainly to the $n = 6$ state corresponding to the angular momentum state $\ell = 0$ in the continuum, which is energetically higher due to the trapping potential $g_h = J$.

regions, defined in Fig. 13(a), after each step of the protocol. As expected, in the first few steps, the number of particles in the LChB $\langle N_{\mathrm{LChB}}\rangle$ increases. However, before the LChB is completely filled, edge states are populated and as a consequence the number of states in HChBs $\langle N_{\mathrm{HChB}}\rangle$ starts to increase. Figure 15(a) shows the population p_n of the first CF states (labeled with integer n) after 25 steps of the protocol.

To avoid population of HChBs, one can stop the protocol when edge states start being populated (i.e., after roughly five steps in Fig. 14). To increase the filling of the LChB further, without populating higher bands, absorbing boundary conditions can be used. Local losses destroy the incompressibility of the state. Repeating the protocol and introducing absorbing boundaries allows to drive the system to its quasistationary state. Since edge states are localized at the boundaries of the system, the bulk properties of the system will only slightly be affected due to the presence of a loss mechanism at the boundary of the system. However, for a properly chosen decay rate γ_{Edge} on the boundary, edge excitations will be lost before they reach the HChB during the protocol. In Fig. 15(b), we show the population of the first CF states after 35 steps of the protocol. The HChBs are only very weakly populated due to the absorbing boundary conditions. The CF density ρ^* of the last cycle is shown in Fig. 1. In terms of the CFs, we reach an average CF filling factor of $\nu^* \simeq 0.9$ of the LChB, which is close to the optimal value $\nu^* = 1$.

V. SUMMARY AND OUTLOOK

In conclusion, we discussed a protocol that allows to grow topologically ordered states in interacting many-body systems. We explained all necessary ingredients using the SLBHM as a simple toy model. We showed that in the flat-band limit a combination of a topologically protected Thouless pump [16,17], creating a local hole excitation, and a coherent pump, refilling the hole excitation, are sufficient. Moreover,

we extended the protocol to the case of dispersive bands and finite systems with edges.

Furthermore, we discussed the protocol in detail in both, the continuum case and the lattice case of fractional quantum Hall systems. In the continuum, we estimated the fidelity of the protocol depending on the particle number N. To describe numerically large lattice systems with many particles, we introduced an effective model based on the CF description of the FQHE. This allows us to simulate large systems and include edge effects. We showed, that a quasihole trapping potential can be used in the case of dispersive bands to maintain a high efficiency of the protocol. Moreover, absorbing boundaries are used in finite systems, where edge states would transport excitations to higher bands. We showed that in the case of dispersive bands and even in the presence of edge states, a high CF filling factor $\nu^* \simeq 0.9$ is achievable, in large systems with more than ten particles.

We believe, that our protocol can be used to grow other exotic states than the LN state, e.g., the Moore-Read Pfaffian [5]. So far, we did not consider experimental realizations. However, ultracold gases as well as photonic systems are promising candidates. Moreover, the efficiency of our scheme can be increased by introducing multiple pairs of topological and coherent pumps.

ACKNOWLEDGMENTS

The authors would like to thank M. Hafezi and L. Glazman for stimulating discussions. F.G. and F.L. are recipients of a fellowship through the Excellence Initiative (DFG/GSC 266). F.G. is grateful for financial support from the "Marion Köser Stiftung."

APPENDIX A: FLUX INSERTION IN THE IQHE

To address the problem of flux insertion, we briefly review the Landau Level (LL) problem. To this end, we use a basis, which is not typically used in standard textbooks. It will turn out that this basis allows a simple understanding of the flux insertion process.

1. Landau level

The LL Hamiltonian in symmetric gauge, $\boldsymbol{A} = B/2(-y,x,0)$, is ($\hbar = 1$)

$$\hat{\mathcal{H}}_0 = \frac{1}{2M}(\boldsymbol{p}-\boldsymbol{A})^2 = \frac{1}{2M}\boldsymbol{p}^2 + \frac{1}{2}M\left(\frac{\omega_c}{2}\right)^2(x^2+y^2) - \frac{\omega_c}{2}L_z. \quad \text{(A1)}$$

As angular momentum L_z is a conserved quantity, i.e., $[\hat{\mathcal{H}}_0, L_z] = 0$, we can use the eigenbasis $|n_r,\ell_r\rangle$ of a two-dimensional harmonic oscillator. Here, $n_r = 0,1,\ldots$ corresponds to the energy levels of the harmonic oscillator and $\ell_r \in \mathbb{Z}$ to those of the angular momentum. We obtain

$$L_z|n_r,\ell_r\rangle = \ell_r|n_r,\ell_r\rangle, \quad \text{(A2)}$$

$$\hat{\mathcal{H}}_0|n_r,\ell_r\rangle = \frac{\omega_c}{2}(2n_r + |\ell_r| - \ell_r)|n_r,\ell_r\rangle. \quad \text{(A3)}$$

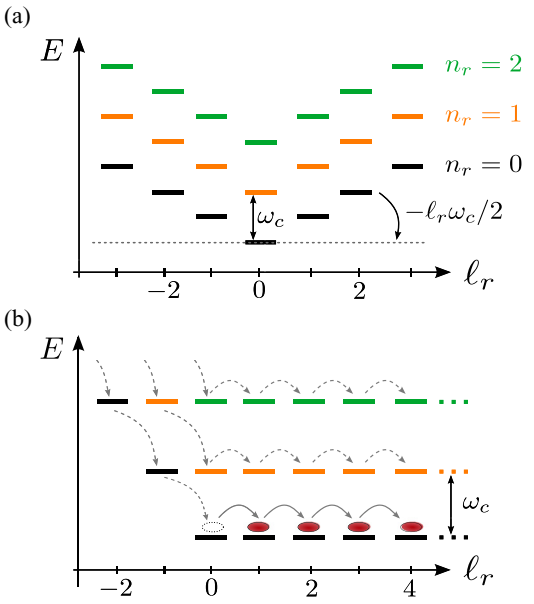

FIG. 16. (Color online) (a) Schematic picture of the LL construction using the two-dimensional harmonic oscillator basis $|n_r,\ell_r\rangle$. (b) In the flux insertion process, the angular momentum ℓ_r is increased by one, while keeping the quantum number n_r fixed.

The energy spectrum of both, the harmonic oscillator and the LL, are shown in Fig. 16.

2. Flux insertion

In 1981, Laughlin [24] explained the quantization of the Hall current using the argument of flux insertion. This idea can be used to create localized hole excitations in the quantum Hall effect. The idea is as follows. After introducing one flux quantum ϕ_0 adiabatically in the center, a circular electric field is generated. The Hall response thus leads to a radial outwards current creating a hole in the center of the system. As shown below, the quasihole excitation is quantized.

To realize Laughlin's argument, we include in Eq. (A1) the vector potential

$$\boldsymbol{A}_\phi = -\frac{\phi(t)}{2\pi r}\boldsymbol{e}_\varphi. \quad \text{(A4)}$$

Defining a new angular momentum

$$L_z^{'} = L_z + \phi/\phi_0, \quad \text{(A5)}$$

we obtain the same structure as in Eq. (A1). However, by adiabatically increasing $\phi(t)$, we change the angular momentum of the system. By inserting one flux quantum ϕ_0, we increase the angular momentum ℓ_r of all states by one, while the quantum number n_r stays fixed. This generates the spectral flow depicted in Fig. 16(b).

APPENDIX B: NONADIABATIC CORRECTIONS IN THE FLUX INSERTION PROCESS

To calculate the probability P_ϕ of exciting particles to higher LLs during flux insertion in the noninteracting case,

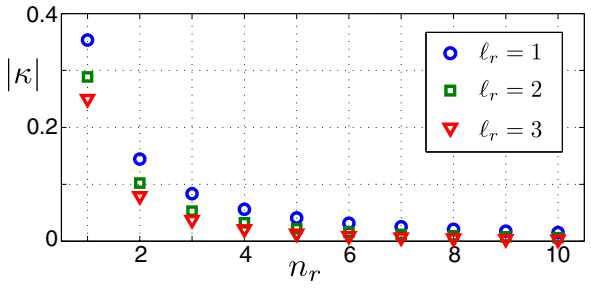

FIG. 17. (Color online) Coupling $|\kappa|$ from the lowest LL $n_r' = 0$ to higher LLs n_r for different angular momentum ℓ_r.

we use the basis discussed in Appendix A. By inserting adiabatically one flux quantum $\phi(t) = \phi_0\, t/T_\phi$ in time $T_\phi \gg 1/\omega_c$, the angular momentum $\ell_r(t)$ increases by one, i.e., $\ell_r(T_\phi) = \ell_r(0) + 1$. Therefore, starting from state $|n_r, \ell_r(0)\rangle$, we end in the state $|n_r, \ell_r(0) + 1\rangle$. Here, we calculate perturbatively in the regime $(\omega_c T_\phi)^{-1} \ll 1$ the scaling of the probability P_ϕ of exciting particles to higher LLs.

The nonadiabatic coupling g_ϕ between different LLs $n_r \neq n_r'$ is

$$\begin{aligned} g_\phi &= \langle n_r', \ell_r| - i\,\partial_t |n_r, \ell_r\rangle \\ &= \langle n_r', \ell_r| - i\,\partial_{\ell_r} |n_r, \ell_r\rangle / T_\phi = \kappa / T_\phi. \end{aligned} \tag{B1}$$

In Fig. 17, we plot the coupling $|\kappa|$ from the lowest LL $n_r' = 0$ to higher LLs n_r for different angular momentum ℓ_r. As expected, the coupling to higher LLs decreases.

To estimate the scaling of P_ϕ with flux insertion time T_ϕ in the perturbative regime $(\omega_c T_\phi)^{-1} \ll 1$, we consider a simple two level approximation with LLs $n_r, n_r + 1$ and constant coupling κ. Starting from the state $|n_r, \ell_r\rangle$, we calculate in first order perturbation theory the probability for ending in state $|n_r + 1, \ell_r\rangle$. We obtain approximately

$$P_\phi \simeq \frac{\kappa^2}{(\omega_c T_\phi)^2} 2(1 - \cos(\omega_c T_\phi)). \tag{B2}$$

We expect, that the scaling of P_ϕ with T_ϕ in the interacting case to be the same as in the noninteracting case, when the cyclotron frequency ω_c is replaced by the many-body gap Δ_{LN}. This leads to Eq. (22).

APPENDIX C: NONADIABATIC CORRECTIONS IN THE COHERENT PUMP PROCESS

In zeroth order in $\Omega/\Delta_{\mathrm{LN}} \ll 1$, the coherent pump couples the quasihole state $|\mathrm{qh}\rangle$ with N particles to the LN state with $N + 1$ particles. The Rabi frequency is Ω and we choose a driving frequency $\omega_c/2$, resonant with the zero-interaction energy LN state $|\mathrm{LN}\rangle$. Thereby, in the continuum, no total angular momentum ΔL_z is transferred.

To first order in $\Omega/\Delta_{\mathrm{LN}}$, we couple the quasihole state $|\mathrm{qh}\rangle$ and the LN state $|\mathrm{LN}\rangle$ to the excitonic states in different particle number sectors from $N - 1$ to $N + 2$, as illustrated schematically in Fig. 18. Here, $|N\rangle_j$ denotes the jth excitonic state in the N particle number sector with many-body gap $\Delta_j^{(N)} \geqslant \Delta_{\mathrm{LN}}$. The effective Rabi frequencies Ω_{ij}, which include the many-body Franck-Condon factors, are labeled by an index $i = 1, \ldots, 4$ as shown in Fig. 18.

For the continuum model discussed in Sec. III, we find, that the Franck-Condon factors

$$\Omega_{2j}/\Omega = {}_j\langle N|\hat{b}_{0,0}|\mathrm{LN}\rangle = 0, \tag{C1}$$

$$\Omega_{3j}/\Omega = {}_j\langle N-1|\hat{b}_{0,0}|\mathrm{qh}\rangle = 0 \tag{C2}$$

vanish. We calculate the excitation probability P_Ω of excitonic states perturbatively to first order in $\Omega/\Delta_{\mathrm{LN}} \ll 1$. Starting from the quasihole state $|\mathrm{qh}\rangle$, after a π pulse of duration $T_\Omega = \pi/2\Omega$, we obtain the result in Eq. (22). There, the factor σ_N is defined as

$$\sigma_N^2 = \left(\frac{\pi}{2}\right)^2 \sum_j \left(\frac{\Omega_{1j}^2/\Omega^2}{\Delta_j^{(N+1)2}/\Delta_{\mathrm{LN}}^2} + \frac{\Omega_{4j}^2/\Omega^2}{\Delta_j^{(N+2)2}/\Delta_{\mathrm{LN}}^2} \right). \tag{C3}$$

We calculated the factor σ_N for different particle numbers N in Fig. 7.

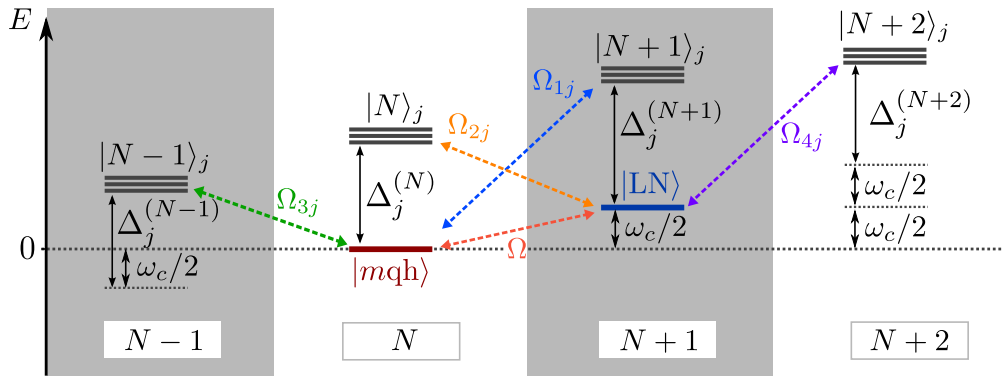

FIG. 18. (Color online) Schematic overview over the coupling between states in different particle number sectors in first order in $\Omega/\Delta_{\mathrm{LN}}$. Starting from the quasihole state $|\mathrm{qh}\rangle$ of N particles or the LN state $|\mathrm{LN}\rangle$ with $N + 1$ particles, the particle number sectors from $N - 1$ to $N + 2$ are involved. Ω_{ij} denotes the many-body Rabi frequencies reduced by their Franck-Condon factors with respect to the bare Rabi frequency Ω. The many-body gaps $\Delta_j^{(N)} \geqslant \Delta_{\mathrm{LN}}$ to the excitonic states $|N\rangle_j$ in the N particle number sector are multiples of the LN gap Δ_{LN}.

[1] K. V. Klitzing, G. Dorda, and M. Pepper, Phys. Rev. Lett. **45**, 494 (1980).
[2] D. C. Tsui, H. L. Stormer, and A. C. Gossard, Phys. Rev. Lett. **48**, 1559 (1982).
[3] D. Arovas, J. R. Schrieffer, and F. Wilczek, Phys. Rev. Lett. **53**, 722 (1984).
[4] B. I. Halperin, Phys. Rev. Lett. **52**, 1583 (1984).
[5] G. Moore and N. Read, Nucl. Phys. B **360**, 362 (1991).
[6] C. Nayak, S. H. Simon, A. Stern, M. Freedman, and S. Das Sarma, Rev. Mod. Phys. **80**, 1083 (2008).
[7] M. Aidelsburger, M. Atala, M. Lohse, J. T. Barreiro, B. Paredes, and I. Bloch, Phys. Rev. Lett. **111**, 185301 (2013).
[8] H. Miyake, G. A. Siviloglou, C. J. Kennedy, W. C. Burton, and W. Ketterle, Phys. Rev. Lett. **111**, 185302 (2013).
[9] G. Jotzu, M. Messer, R. R. Desbuquois, M. Lebrat, T. Uehlinger, D. Greif, and T. Esslinger, Nature (London) **515**, 237 (2014).
[10] M. Aidelsburger, M. Lohse, C. Schweizer, M. Atala, J. T. Barreiro, S. Nascimbène, N. R. Cooper, I. Bloch, and N. Goldman, Nat. Phys. **11**, 162 (2015).
[11] M. Hafezi, S. Mittal, J. Fan, A. Migdall, and J. M. Taylor, Nat. Photon. **7**, 1001 (2013).
[12] M. C. Rechtsman, J. M. Zeuner, Y. Plotnik, Y. Lumer, D. Podolsky, F. Dreisow, S. Nolte, M. Segev, and A. Szameit, Nature (London) **496**, 196 (2013).
[13] R. O. Umucalilar and I. Carusotto, Phys. Rev. Lett. **108**, 206809 (2012).
[14] E. Kapit, M. Hafezi, and S. H. Simon, Phys. Rev. X **4**, 031039 (2014).
[15] F. Grusdt, F. Letscher, M. Hafezi, and M. Fleischhauer, Phys. Rev. Lett. **113**, 155301 (2014).
[16] D. J. Thouless, Phys. Rev. B **27**, 6083 (1983).
[17] D. J. Thouless, M. Kohmoto, M. P. Nightingale, and M. Den Nijs, Phys. Rev. Lett. **49**, 405 (1982).
[18] R. Shindou, J. Phys. Soc. Jpn **74**, 1214 (2005).
[19] E. Berg, M. Levin, and E. Altman, Phys. Rev. Lett. **106**, 110405 (2011).
[20] P. Buonsante, V. Penna, and A. Vezzani, Phys. Rev. A **70**, 061603(R) (2004).
[21] P. Buonsante and A. Vezzani, Phys. Rev. A **70**, 033608 (2004).
[22] P. Buonsante and A. Vezzani, Phys. Rev. A **72**, 013614 (2005).
[23] D. Muth, A. Mering, and M. Fleischhauer, Phys. Rev. A **77**, 043618 (2008).
[24] R. B. Laughlin, Phys. Rev. B **23**, 5632 (1981).
[25] F. Grusdt, M. Höning, and M. Fleischhauer, Phys. Rev. Lett. **110**, 260405 (2013).
[26] A. R. Kolovsky, F. Grusdt, and M. Fleischhauer, Phys. Rev. A **89**, 033607 (2014).
[27] *The Quantum Hall Effect*, edited by R. E. Prange and S. M. Girvin, 2nd ed. (Springer-Verlag, Berlin, 1990).
[28] J. K. Jain, *Composite Fermions* (Cambridge University Press, Cambridge, 2007).
[29] S. A. Trugman and S. Kivelson, Phys. Rev. B **31**, 5280 (1985).
[30] N. K. Wilkin, J. M. F. Gunn, and R. A. Smith, Phys. Rev. Lett. **80**, 2265 (1998).
[31] N. K. Wilkin and J. M. F. Gunn, Phys. Rev. Lett. **84**, 6 (2000).
[32] N. R. Cooper and N. K. Wilkin, Phys. Rev. B **60**, R16279(R) (1999).
[33] N. Regnault and T. Jolicoeur, Phys. Rev. Lett. **91**, 030402 (2003).
[34] N. Regnault and T. Jolicoeur, Phys. Rev. B **69**, 235309 (2004).
[35] B. A. Bernevig and F. D. M. Haldane, Phys. Rev. Lett. **100**, 246802 (2008).
[36] S. Zhang, T. Hansson, and S. Kivelson, Phys. Rev. Lett. **62**, 980 (1989).
[37] N. Read, Phys. Rev. Lett. **62**, 86 (1989).
[38] J. K. Jain, Phys. Rev. Lett. **63**, 199 (1989).
[39] F. D. M. Haldane, Phys. Rev. Lett. **51**, 605 (1983).
[40] C. Brouder, G. Panati, M. Calandra, C. Mourougane, and N. Marzari, Phys. Rev. Lett. **98**, 046402 (2007).
[41] M. Hafezi, Phys. Rev. Lett. **112**, 210405 (2014).
[42] B. Paredes, P. Fedichev, J. I. Cirac, and P. Zoller, Phys. Rev. Lett. **87**, 010402 (2001).
[43] G. Nandi, R. Walser, and W. P. Schleich, Phys. Rev. A **69**, 063606 (2004).
[44] M. F. Andersen, C. Ryu, P. Cladé, V. Natarajan, A. Vaziri, K. Helmerson, and W. D. Phillips, Phys. Rev. Lett. **97**, 170406 (2006).
[45] A. S. Sørensen, E. Demler, and M. D. Lukin, Phys. Rev. Lett. **94**, 086803 (2005).
[46] M. Hafezi, A. S. Sørensen, M. D. Lukin, and E. Demler, Europhys. Lett. **81**, 10005 (2008).
[47] G. Möller and N. R. Cooper, Phys. Rev. Lett. **103**, 105303 (2009).
[48] T. Liu, C. Repellin, B. A. Bernevig, and N. Regnault, Phys. Rev. B **87**, 205136 (2013).